International Journal of Advancements in Mechanical and Aeronautical Engineering– IJAMAE
Volume 1: Issue 2 *[ISSN 2372-4153]*
Publication Date : 25 June 2014

Aerodynamic Performance of Twist Morphing MAV Wing

N.I. Ismail , A.H. Zulkifli , M.Z. Abdullah, M.Hisyam Basri and Norazharuddin Shah Abdullah

***Abstract*—Twisted wing (TW) is a morphing technique that particularly suitable for a membrane wings MAV. However, the aerodynamic advantages of TW application on MAV wing scale are still needed to be explored. This is because the MAV design challenge is still concentrated in generating enough lift during flight. Thus, the present research is carried out to acquire an understanding of the basic aerodynamic performance of a TW MAV design. Based on fluid structure interaction (FSI) simulation, a comparative study with the baseline membrane and rigid wing performances is carried out to elucidate the superiority of the morphing wing lift and drag performance. The results show that, the TW configuration has significantly produced the highest CL and CD distribution. At a certain angle of attack (AOA), the TW configuration can generate up to 200% better CL than to the other wing types. However, TW also produced significantly higher drag than to the other wings. This drag results has overwhelm the successive increase in lift generation and consequently plunge the overall TW aerodynamic efficiency.**

Keywords—Fluid structure interaction; micro air vehicle; twist morphing wing.

I. Introduction

A micro aerial vehicle (MAV) is defined as a micro-scale aircraft (maximum wingspan of 15 cm). It has a huge potential to replace the unmanned aerial vehicle (UAV) for confined space operational areas i.e. indoor and between buildings. Rigid-wing MAV types is very popular in the early works of MAV generation. However, due to its low aspect ratio configuration, it causes large wing tip vortex swirling[1], difficult flight controllability[2], and small center of gravity range[3].

N.I. Ismail
Faculty of Mechanical Engineering, Universiti Teknologi MARA Malaysia

A.H. Zulkifli
Faculty of Mechanical Engineering, Universiti Teknologi MARA Malaysia

M.Z. Abdullah
School of Mechanical Engineering, Universiti Sains Malaysia, Engineering Campus, Malaysia

M.Hisyam Basri
Faculty of Mechanical Engineering, Universiti Teknologi MARA Malaysia

Norazharuddin Shah Abdullah
School of Materials and Mineral Resources Engineering, Universiti Sains Malaysia, Engineering Campus, Malaysia

Therefore, evolution of MAV generation is introduced based on biological inspired design through passive wing (also known as membrane wing design)[4], [5] and active wing designs (also known as morphing wing design)[6]. The morphing technique has been naturally used by insects, birds and flying mammals in flight maneuvering method. Morphing is a certain technique that embedded into a wing which has capabilities to change its shape during flight[7]. Chord length changes, swept angle variation, or spanwise or chordwise wing warping[8] are a common example of morphing wing. Twisted wing (TW) is also another morphing method that has been introduced as a practical control technique in MAV flight dynamics[6]. TW is particularly suitable for a membrane wings MAV since it can be morphed with minimum power and produced a significant control authority for lateral dynamics[6]. However, the aerodynamic advantages of TW application on MAV wing scale are still needed to be explored. This is because the main challenge in MAV wing design is still focusing to produce enough lift during flight[8].

Thus, the present research is carried out to acquire an understanding of the basic aerodynamic performance of a TW MAV design, particularly on its lift and drag distribution. A comparative study with the baseline membrane and rigid wing performances are carried out to elucidate the superiority of the morphing wing aerodynamic performance. In this preliminary study, the numerical fluid structure interaction (FSI) method based on ANSYS commercial software is utilized.

II. FSI computation method

In the present research, FSI method is used to study quasi-static TW MAV wing performance. To solve the turbulent flow issue, 3D RANS equations coupled with SST k-ω turbulent equation are employed under the assumption of a steady, incompressible, and turbulent airflow field. The FSI coupling technique also includes static-based structural wing deformation. A strong coupled FSI simulation process[9] is summarized in **Fig 1**.

A. MAV wing models

In the present research, the TW, membrane and rigid MAV wings are modeled in ANSYS Mechanical-CFX FSI simulation. Summary of the basic design dimension and configuration for all wing types is given in **Table 1**. As shown in **Fig. 2**, all wing configurations used in this study are almost identical in terms of platform shape and dimension. The wings differ in morphing force and flexible membrane skin components.

The TW has baseline membrane wing characteristics with additional morphing force component at the wing underneath. The force component is located at an optimized position on the wingtip (90 mm from the leading edge and parallel to the wing spanwise axis). The morphing force is enforced at 5 N and

directed at 45° from the XZ plane. Technically, the objective function of this total morphing force is to produce the wingtip y-direction displacement magnitude and directly create a twisted motion on the TW model. The physical structure and basic kinematic principle of a TM wing mechanism are shown in **Fig. 3**.

The thickness (including the membrane skins) for all wing models is set at 1.0 mm. The following coordinate system is adopted: x is chordwise direction, z is spanwise direction, and y is normal to the wing, with the origin located at the wing leading edge.

B. *Material selection and mesh generation for static structural analysis*

Polymethyl methacrylate (also known as Perspex) and rubber are utilized for the wing skeleton and membrane skin of the wings, respectively. Isotropic, homogeneous, and linearly elastic characteristics are assumed for all materials considered. The material properties of Perspex and rubber are listed in **Table 2**. Instead of a hyperelasticity material model, a linear elastic model is used for the rubber material for simplification[10]. Unstructured tetrahedral mesh with ANSYS SOLID 187 3D element type is created for all wing models. Results of the grid independent study on an optimized grid around 116,000 elements for static structural analysis are shown in **Fig. 4**.

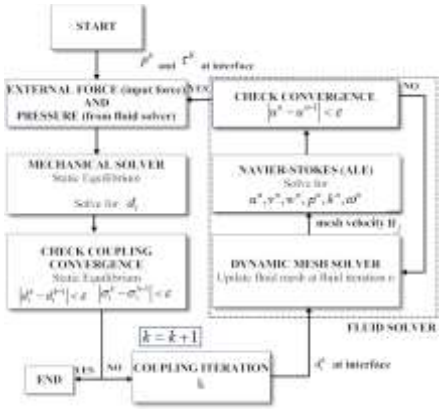

Figure 1. FSI simulation process.

TABLE 1. BASIC DESIGN DIMENSION AND CONFIGURATION FOR ALL MAV WING TYPES.

	TW	Membrane wing	Rigid wing
Wingspan, b	150mm	150mm	150mm
Root chord, c	150mm	150mm	150mm
Aspect ratio, A	1.25	1.25	1.25
Maximum camber at the root	6.7% of c (at x/c =0.3)	6.7% of c (at x/c = 0.3)	6.7% of c (at x/c =0.3)
Maximum reflex at the root	1.4% of c (at x/c = 0.86)	1.4% of c (at x/c = 0.86)	1.4% of c (at x/c =0.86)
Built-in geometric twist	0.6°	0.6°	0.6°
Force component	Included F=5N	Excluded	Excluded
Membrane skin	Included	Included	Excluded

C. *Flow domains and mesh generation*

The computational flow domain (CFD) is built around an MAV wing, in which the symmetrical condition is manipulated by modeling only half of the computational domain. As shown in **Fig. 5**, the 3D boundary of the CFD is dimensioned in the root chord unit(c), and placed remotely from the MAV surface to ensure that no significant effect is applied on aerodynamics. An initial model with 200,000 unstructured elements is created and used to solve the airflow field issue. Grid-independent test results show that the optimized grid is achieved at 1,000,000 elements as depicted in **Fig. 6**. The growing prism inflation layer option is implemented on fluid–solid boundaries with the first cell above the wall set at $y^+ \leq 1$.

The inlet and outlet are marked by flow vectors (**Fig. 5**). The magnitudes of velocity are set at 9.5m/s which is equivalent to Reynolds number (Re) =100,000 at chord). Inlet velocity is specified at the inlet, and zero pressure boundary condition is enforced at the outlet. The angle of attack (AOA) of the wing varies from -10° to 35°. Symmetrical and side walls are assigned as symmetrical and slip surface boundary conditions, respectively. The wing surface is modeled as a no-slip boundary surface and assigned as the boundary interaction for FSI investigation. Automatic wall function is fully employed to solve the flow viscous effect.

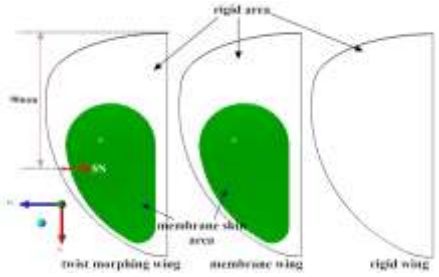

Figure 2. Wing configurations as viewed from the bottom angle.

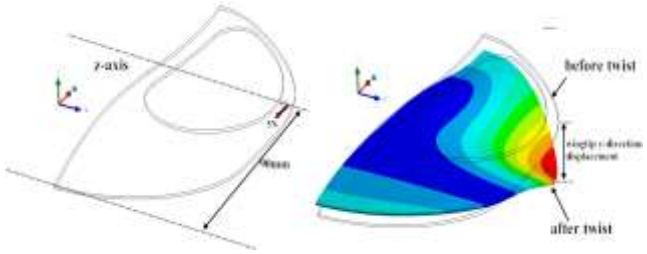

Figure 3. Physical structure and basic kinematic principle of a TW mechanism.

TABLE 2.MATERIAL PROPERTIES OF PERSPEX AND RUBBER.

Material Name	Density (kg/m^3)	Young Modulus (Pa)	Poisson`s Ratio	Bulk Modulus (Pa)	Shear Modulus (Pa)	Tensile Yield Strength (Pa)
Perspex (Polymethyl methacrylate)	1190	$2.8x10^9$	0.46	$1.667x10^{10}$	$9.589x10^8$	70
Rubber	1000	$8.642x10^6$	0.49	$1.44x10^8$	$2.9x10^6$	$1.3787x10^7$

Figure 4. Elements for static structural analysis of a TM wing.

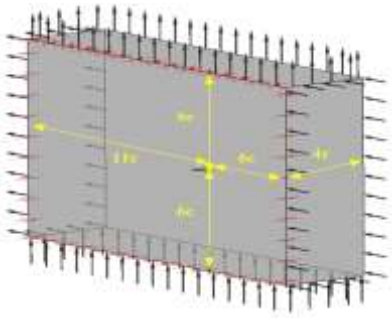

Figure 5. Computational flow domain.

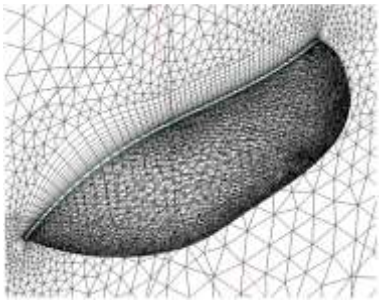

Figure 6. Elements for CFD analysis.

III. Results

A. *Validation of FSI simulation method*

A validation work has been conducted to compare the FSI simulation and experimental results which has been carried out at Aerodynamic Laboratory, School of Mechanical Engineering, Universiti Sains Malaysia. **Fig.7** presents the lift (CL) and drag coefficient (CD) validation data for TW at 9.5 m/s (Re≈100,000). It apparently shows that the lift and drag simulation curves remain very close to the experimental data starting from low AOA (-10°) up to the stall angle (AOA≈15°). A slight discrepancy is illustrated in this AOA region, and the significant increment trend is captured by the simulation curve. As the AOA increases beyond the stall angle, the simulation curve begins to drop at magnitude lower than the experimental value. This finding may be attributed to higher turbulent phenomenon and organized transient motion at the post stall angle, which might not be sufficiently predicted by the RANS SST *k*-ω turbulent model[11], [12]. Despite this discrepancy, the overall trend of CL and CD performance toward AOA increment is satisfactorily captured by the FSI simulation. The simulation results also show a strong correlation with experimental results at the AOA region below the stall angle. This condition signifies that the FSI simulation possesses high predicting capability to calculate the lift and drag distribution at this certain sweep angle region. Therefore, the FSI simulation results are justified for further analysis.

B. *Lift and drag distribution pattern*

Investigations on CL pattern on all wing configurations are depicted in **Fig. 8**. At this point, the CL for every wing has performed nonlinearly with AOA changes. This is common lift characteristic for low aspect ratio wings suggested by previous works, e.g. by Shields et al.[13], Mueller[14], Pelletier et al.[15], Sathaye[16] and Mueller et al.[17]. In evaluating these nonlinear lift performance, TW configuration has surprisingly produced better lift distribution compared with the membrane or rigid wing. Analytically, the TW has an ability to generate up to 200% better lift than to the other wings at AOA below 2°. However, these advantages are monotonically decreased as the AOA increase towards TW's stall angle (AOA=14°). After stall angle, the CL of TW tends to drop at magnitude lower than the other wing's CL. Moreover, TM also promotes stall conditions earlier than the membrane or rigid wing. This situation is resulting from the increment of local wing incidence known as twist or wash-in wing effect[18].

The drag distribution pattern for all wing configurations is presented in **Fig. 9**. For AOA region below 0°, the magnitude of CD for all wings performs almost similarly. As the AOA increases higher than 0°, the TW configuration emerges as the highest drag generators among all wings. Analytically, the TW has an ability to generate up to 200% more drag than to the other wings at AOA below 10°. This percentage is decreased as the AOA increase further, but the magnitude still remains higher than 40%. Based on these results, it is concluded that TW is significantly suffered from larger drag penalty than the other wings. This situation has a close connection to the strong TV formation on low aspect ratio wing discussed in reference [13], [19].

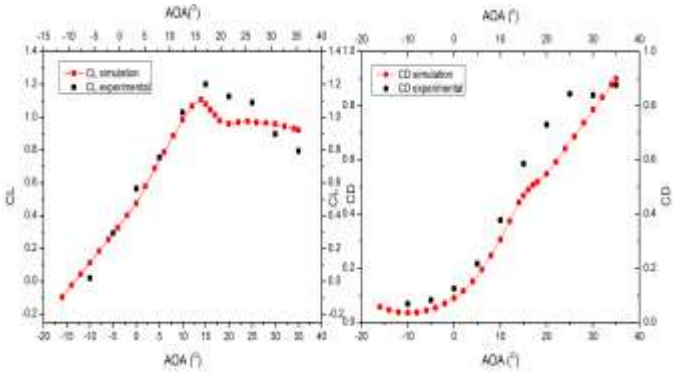

Figure 7. Validation of lift (left) and drag coefficient (right) on TW wing at 9.5 m/s.

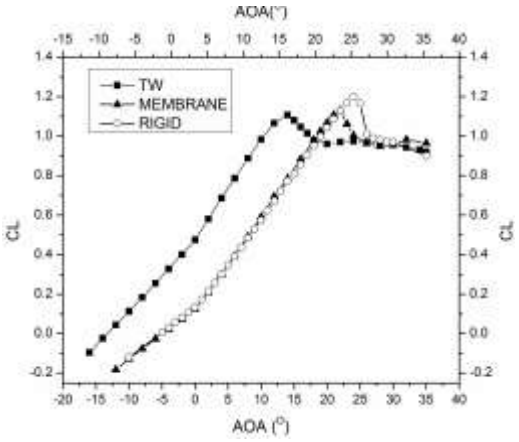

Figure 8. The CL distribution for all wing configurations

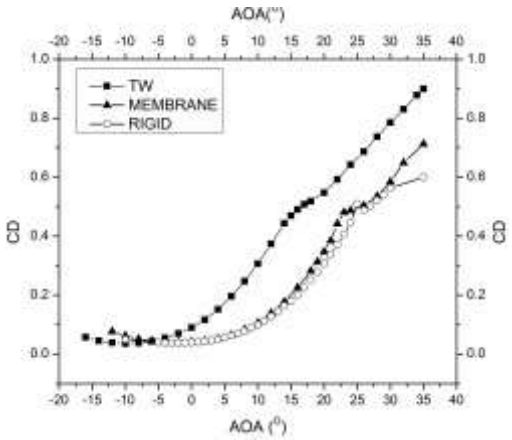

Figure 9. The CD distribution for all wing configurations.

C. *Aerodynamic efficiency*

The lift to drag ratio (CL/CD) for all wings are given as a function of CL in **Fig.10**. In aerodynamic study, CL/CD is always used to signify the performance of wing aerodynamic efficiency. **Fig.10** shows that all wings perform almost similarly at CL below 0.2. However, as CL increase more than 0.2, the CL/CD curve for TW begins to deviate, giving lower CL/CD values, compared to membrane or rigid wing curve. The peak efficiency for TW wing is achieved at CL/CD_{TW}= 6.05, which is 4.5% lower than rigid wing's peak efficiency (CL/CD_{RIGID}= 6.32). Moreover, the peak efficiency of TW occur at lower angle (AOA=-4°) compares to membrane or rigid wing (AOA=6°).

Based on this aerodynamic efficiency performance, one can presume that TW wing has a lower aerodynamic efficiency compares to membrane or rigid wing. Shyy et al.[20] and Stanford et al.[21] suggested that the plunge of aerodynamic efficiency for membrane wing MAV (i.e. TW and membrane wing in current case study) is most probably due to massive drag penalty created on, in which has overwhelms the successive increase in lift generation.

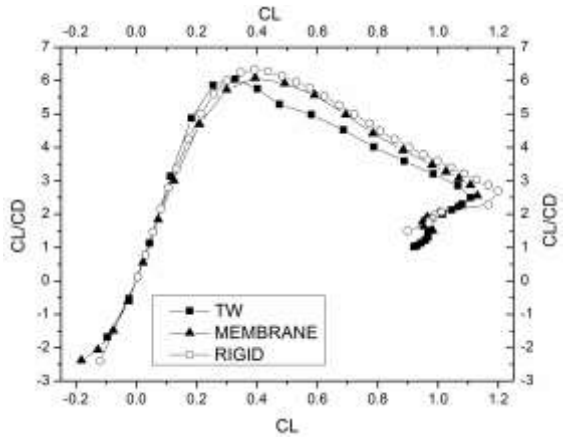

Figure 10. Aerodynamic efficiency for all wing configurations.

IV. Conclusion and future works

A two-way FSI simulation consisting 3D incompressible RANS-SST and static structural solver are used to solve the wing aerodynamics for a steady, incompressible flow over TW, membrane and rigid wings. In this numerical study, the TW wing is actuated with 5N force to activate the twist morphing effect. Membrane and rigid wings are also included in the analysis for comparative study.

The early validation results show that the FSI simulation and selected experimental results are consistent, particularly at the AOA region below the stall angle. The overall lift and drag distribution patterns are sufficiently captured and predicted by the FSI simulation. In CL study, the TW configuration has significantly produces the highest CL and CD distribution. At AOA below 2°, TW configuration has an ability to generate up to 200% better CL than to the other wings. However, TW also malevolently produced higher drag than to the other wings especially at AOA below 10°. This drag results has overwhelm the successive increase in lift generation and consequently plunge the overall TW aerodynamic efficiency.

Future work will include the variation of force for TW activation with its experimental validation on the aeroelastic wing deformation and flow structures. The optimal aerodynamic efficiency study on TW configuration is also very promising in order to improve this morphing wing type.

Acknowledgment

The authors acknowledge the technical support from Universiti Teknologi MARA and the scholarship by the Ministry of Higher Education under the IPTA Academic Training Scheme awarded to the first author. The financial support provided by the Malaysia Ministry of Higher Education's Fundamental Research Grant Scheme (FRGS) (600-RMI/FRGS5/3 (22/2012)) is also acknowledged.

References

[1] D. Viieru, R. Albertani, W. Shyy, and P. Ifju, "Effect of Tip Vortex on Wing Aerodynamics of Micro Aerial Vehicles," *AIAA Journal*, vol. 42, no. 4, pp. 1530–1536, 2005.

[2] Y. Lian and W. Shyy, "Laminar-Turbulent Transition of a Low Reynolds Number Rigid or Flexible Airfoil," *AIAA Journal*, vol. 45, no. 7, pp. 1501–1513, 2007.

[3] R. Albertani, B. K. Stanford, J. P. Hubner, and P. G. Ifju, "Aerodynamic Coefficients and Deformation Measurements on Flexible Micro Air Vehicle Wings," *Experimental Mechanics*, vol. 47, no. 5, pp. 625–635, Feb. 2007.

[4] B. K. Stanford, P. Ifju, R. Albertani, and W. Shyy, "Fixed Membrane Wings For Micro Air Vehicles: Experimental Characterization, Numerical Modeling, And Tailoring," *Progress in Aerospace Sciences*, vol. 44, no. 4, pp. 258–294, May 2008.

[5] B. K. Stanford, "Aeroelastic Analysis and Optimization of Membrane Micro Air Vehicle Wings," PhD. Thesis Dissertation, University Of Florida, 2008.

[6] M. Abdulrahim, H. Garcia, and R. Lind, "Flight Characteristics of Shaping the Membrane Wing of a Micro Air Vehicle," *Journal Of Aircraft*, vol. 42, no. 1, 2005.

[7] A. Y. N. Sofla, S. A. Meguid, K. T. Tan, and W. K. Yeo, "Shape morphing of aircraft wing : Status and challenges," *Materials and Design*, vol. 31, pp. 1284–1292, 2010.

[8] J. Valasek, Ed., *Morphing Aerospace Vehicles and Structures*. John Wiley & Sons, Ltd., 2012, p. 306.

[9] "ANSYS CFX-Solver Theory Guide," vol. 15317, Canonsburg, PA: ANSYS, Inc., 2010, pp. 724–746.

[10] Y. Lian, W. Shyy, D. Wiieru, B. Zhang, D. Viieru, and A. I. N. Press, "Membrane Wing Aerodynamics For Micro Air Vehicles," *Progress in Aerospace Sciences*, vol. 39, no. 6–7, pp. 425–465, Oct. 2003.

[11] A. . Benim, E. Pasqualotto, and S. H. Suh, "Modelling turbulent flow past a circular cylinder by RANS, URANS, LES and DES," *Progress in Computational Fluid Dynamics, an International Journal*, vol. 8, no. 5, pp. 299–307, 2008.

[12] A. C. Benim, M. Cagan, A. Nahavandi, and E. Pasqualotto, "RANS Predictions of Turbulent Flow Past a Circular Cylinder over the Critical Regime," in *5th IASME / WSEAS International Conference on Fluid Mechanics and Aerodynamics*, 2007, pp. 232–237.

[13] M. Shields and K. Mohseni, "Effects of Sideslip on the Aerodynamics of Low-Aspect-Ratio," *AIAA Journal*, vol. 50, no. 1, pp. 85–99, 2012.

[14] T. J. Mueller, "Aerodynamic Measurements at Low Reynolds Numbers for Fixed Wing Micro-Air Vehicles," 1999.

[15] A. Pelletier, T. J. Mueller, and N. Dame, "Low Reynolds Number Aerodynamics of Low-Aspect-Ratio , Thin / Flat / Cambered-Plate Wings," *Journal Of Aircraft*, vol. 37, no. 5, pp. 825–832, 2000.

[16] S. S. Sathaye, "Lift Distributions on Low Aspect Ratio Wings at Low Reynolds Numbers," MSc Thesis Dissertation, Worcester Polytechnic Institute, 2004.

[17] T. J. Mueller and G. E. Torres, "Aerodynamics of Low Aspect Ratio Wings at Low Reynolds Numbers With Applications to Micro Air Vehicle Design and Optimization," UNDAS-FR-2025, 2001.

[18] R. Vos, Z. Gurdal, and M. Abdalla, "Mechanism for Warp-Controlled Twist of a Morphing Wing," *Journal of Aircraft*, vol. 47, no. 2, pp. 450–457, Mar. 2010.

[19] K. Taira and T. Colonius, "Effect of Tip Vortices in Low-Reynolds-Number Poststall Flow Control," *AIAA Journal*, vol. 47, no. 3, pp. 749–756, Mar. 2009.

[20] W. Shyy, P. Ifju, and D. Viieru, "Membrane Wing-Based Micro Air Vehicles," *Applied Mechanics Reviews*, vol. 58, pp. 283–301, 2005.

[21] B. K. Stanford and P. Ifju, "Membrane Micro Air Vehicles with Adaptive Aerodynamic Twist : Numerical Modeling," *Journal of Aerospace Engineering*, vol. 22, no. 2, pp. 173–184, 2009.